ADVANCED HEALTHCARE MATERIALS
www.advhealthmat.de

Strontium and Tannic Acid-Modified Eggshell-Derived Nanoparticles Promote Wound Healing in Poly(Lactic Acid)/Gelatin-Based Nanofibrous Dressings

Bin Shao, Zhiyu Mu, Zhengchao Yuan, Muhammad Shafiq, Zheng Lei, Hao Feng, Lu Han, Mohamed EL-Newehy, Meera Moydeen Abdulhameed, Jiaojiao Li, Peng Li, Xiumei Mo,* and Weidong Mu**

Wound healing may be impaired by excessive bleeding, bacterial colonization, slower angiogenesis, and poor cell proliferation, which necessitate the advent of innovative hemostatic, antibacterial, and pro-angiogenic dressings. The objective of this research is to synthesize strontium-substituted tannic acid-modified eggshell-based nanoparticles (ECa-TA-Sr NPs) and exploit them to endow multifunctionality to poly(lactic acid)/gelatin (PG) fibers. Physical and chemical properties of unmodified and modified NPs, as well as dressings, are evaluated with different types of assays in vitro. Hemostatic ability as well as wound healing ability of dressings is discerned in a rat liver trauma model and a full-thickness excisional defect model in vivo. Dressings loaded with ECa-TA-Sr NPs exhibit antibacterial activity against *E. coli* and *S. aureus*, anti-inflammatory ability, angiogenic ability, rapid hemostatic ability, and faster wound closure than that of the PG fibers. Therefore, ECa-TA-Sr NPs derived from the eggshell can enable multifunctionality to dressings and may also be worthy for future investigations.

1. Introduction

The skin, as the largest organ of the body, plays a pivotal role along with several functions, such as sensory and secretory function, thermoregulation, barrier against viruses and bacteria, and so on.[1] Different types of factors, such as burns, infections, and large-scale wounds, may damage the skin and lead to its dysfunction, thereby posing aesthetic issues as well as economic burden.[2] Wound healing is a dynamic process, which is composed of various overlapping phases, including hemostasis, inflammation, re-epithelialization, and tissue remodeling.[3] Wounds with slight damage could be repaired by an intrinsic self-healing mechanism of the body. However, chronic wounds or those with a large size may not heal themselves, thereby causing skin tissue necrosis. These wounds require dressings for functional skin repair.[4]

Infections, diabetes, and burn injuries may obscure the natural wound healing mechanism.[5] Moreover, these wounds may accompany bleeding, exaggerated inflammation, and even tissue necrosis.[6] An array of dressings has been used for wound healing, which are generally based on electrospun fibers, three-dimensional (3D) scaffolds, hydrogels, and aerogels.[7] Moreover, different types of nanomaterials (NMs), such as silver nanoparticles (Ag NPs), bioactive glasses (BGs), and other functional NPs,

B. Shao
Shandong University of Traditional Chinese Medicine
Jinan, Shandong 250355, China
B. Shao
Department of Spinal Surgery
Binzhou Medical University Hospital
Binzhou, Shandong 256603, China
Z. Mu, J. Li
School of Biomedical Engineering
Faculty of Engineering and IT
University of Technology Sydney
Ultimo NSW2007, Australia

The ORCID identification number(s) for the author(s) of this article can be found under https://doi.org/10.1002/adhm.202502979

DOI: 10.1002/adhm.202502979

Z. Yuan, Z. Lei, H. Feng, L. Han, X. Mo
State Key Laboratory for Modification of Chemical Fibers and Polymer Materials
Shanghai Engineering Research Center of Nano-Biomaterials and Regenerative Medicine
College of Biological Science and Medical Engineering
Donghua University
Shanghai 201620, China
E-mail: xmm@dhu.edu.cn
M. Shafiq
Innovation Center of NanoMedicine (iCONM)
Kawasaki Institute of Industrial Promotion
Kawasaki-Ku, Kawasaki 2100821, Japan
M. EL-Newehy, M. M. Abdulhameed
Department of Chemistry
College of Science
King Saud University
P.O. Box 2455, Riyadh 11451, Saudi Arabia

are incorporated into dressings owing to their multifunctional characteristics.[8] Previously, the authors' group has synthesized egg shell (ES)-based NPs (abbreviated as ECa NPs). ECa NPs improved skin tissue repair due in part to the release of different types of therapeutic ions, such as calcium ions (Ca^{2+}), magnesium ions (Mg^{2+}), and silicate ions (SiO_3^{2-}). These therapeutic ions can stimulate the coagulation pathway to achieve hemostasis, and they may additionally promote extracellular matrix (ECM) deposition for effective skin tissue repair.[9,10] More importantly, since these ECa NPs are derived from the waste byproduct of the egg from the household industry, they may have considerable promise owing to their cost-effectiveness and easier availability.[11,12]

Despite significant promise of ECa NPs for skin tissue repair, they lack biological functions, such as antibacterial, anti-inflammatory, and immunomodulatory properties.[13] These limitations may hamper the wider applicability of ECa NPs for the treatment of chronic wounds.[14] Bacterial infections may cause tissue necrosis, delay wound healing, and even cause amputation after skin injury.[15] Tannic acid (TA) belongs to the natural polyphenols, and exhibits multivarious advantageous features, such as anti-inflammatory, anti-oxidative, and antibacterial properties.[16] Antibacterial properties of TA can help avoid antibiotic resistance. Despite these advantageous features, TA lacks bioactivity in vivo.[17,18] Moreover, sufficient angiogenesis is also an important factor in wound healing. Therapeutic ions, such as strontium ions (Sr^{2+}), can promote angiogenesis due in part to their cellular metabolism bioactivity.[19] Therefore, TA and Sr^{2+} can be chemically modified onto ECa NPs, which may have implications for antibacterial properties and vasculogenic-inducing abilities of wound dressings in vitro and in vivo (**Figure 1a**).[20]

However, ECa-TA-Sr NPs cannot be directly applied to the wound site due to their poor retention at the injury site.[21] The lack of a stable application form of NPs may also increase the pH and induce cytotoxicity, thereby compromising the wound healing efficacy.[9] The nanofiber scaffolds could be obtained by electrospinning, which display sufficient porosity, suitable mechanical properties, and ECM-like structure.[14] Poly(lactic acid) (PLA) shows good biocompatibility and biodegradability, and is widely used to fabricate scaffold materials. However, PLA exhibits strong hydrophobicity, which could affect the release of bioactive components. Gelatin (Gel) exhibits good hydrophilicity, rapid degradation, and good biocompatibility. Gel has been intensively exploited for tissue engineering (TE) applications.[22]

The objective of this research was to synthesize multifunctional ECa-TA-Sr NPs and incorporate them into PLA/Gel-based fibrous dressings (Figure 1b). While ECa-TA-Sr NPs can exhibit multifunctional characteristics, such as antibacterial, anti-inflammatory, and anti-oxidative properties, PLA/Gel (herein abbreviated as PG) can be prepared into nanofibers and help incorporate ECa-TA-Sr NPs for an effective application form for in vitro and in vivo applications. The ECa-TA-Sr NPs-loaded PG fibers (herein abbreviated as PG-ETS) exhibit ECM-like morphological features with sufficient porosity and pore size. The cytocompatibility and biofunction of dressings were elucidated using different types of assays, including Transwell migration assay, antibacterial activity, and tubule-like network formation of human umbilical vein endothelial cells (HUVECs). Besides, the hemostatic ability of dressings as well as the potential of dressings to improve in situ skin tissue repair was elucidated in a rat liver injury model and a full-thickness excisional defect model (Figure 1c).

2. Results

2.1. Characterizations

The ES is an important source of calcium oxide (CaO), which exhibits 96.4 wt.% calcium carbonate ($CaCO_3$) along with a small amount of other metal salts. In addition to calcium (Ca), ECa NPs also exhibited other components, such as silicon (Si) and magnesium (Mg), as revealed by EDS (Figure S1, Supporting Information). The ES also contains fibrous proteins, including collagen type I (Col I), glycosaminoglycans (GAGs), chondroitin sulfate (CS), hexosamines, and partial pigmenting substances. The ES exhibited yellow-brown colour with a certain brittleness (**Figure 2a**). It is worth noting that depending upon the different ratios of protoporphyrin and biliverdin, the ES derived from different sources may exhibit different colours. The ES was ground at high temperature to form a white-colored powder. During the calcination process, organic components, including pigments, can be removed, while inorganic components can be converted into their respective oxides. ECa NPs loaded with TA and TA-Sr displayed yellow and light gray colours, respectively (Figure 2a). The morphological analysis revealed that the ES was lumpy, while ECa, ECa-TA, and ECa-TA-Sr were granular with an irregular morphology (Figure 2b).

These particles have good dispersibility, which can be easily dispersed into the PG spinning solution and form a stable turbid suspension (Figure S2a, Supporting Information). While PG and PG-E spinning solutions were colorless, transparent, and milky, PG-ET and PG-ETS spinning solutions displayed light yellow and light gray colours, respectively (Figure S2, Supporting Information). Fibrous dressings containing different types of NPs did not significantly differ in terms of the visual appearance, which may be ascribed to the dispersion of NPs in PG fibers (Figure S2, Supporting Information). Moreover, fibrous dressings exhibited ECM-like morphology along with micropores among fibers (Figure 2c).

The pore size of PG-ETS was in the range of 0.8–3.2 µm, and the average pore size was 1.79 µm (Figure S3, Supporting Information). Average fiber diameter was 0.67 ± 0.07 µm, 0.69 ± 0.06 µm, 0.74 ± 0.06 µm, and 0.72 ± 0.07 µm for PG, PG-E, PG-ET, and PG-ETS groups, respectively. These data showed that the incorporation of NPs into PG can increase the diameter of the fibers (Figure 2e–h). Moreover, the values of water contact angle (WCA) were 49.9 ± 2.3°, 47.2 ± 1.5°, 38.5 ± 1.4°, and 33.1 ± 1.8° for PG, PG-E, PG-ET, and PG-ETS groups, respectively, which is

P. Li
Department of Orthopedic Trauma
Binzhou Medical University Hospital
Binzhou, Shandong 256603, China
E-mail: lpcsgk@126.com
W. Mu
Department of Traumatic Orthopaedics
Shandong Provincial Hospital
Jinan, Shandong 250021, China
E-mail: sdslyymwd@126.com

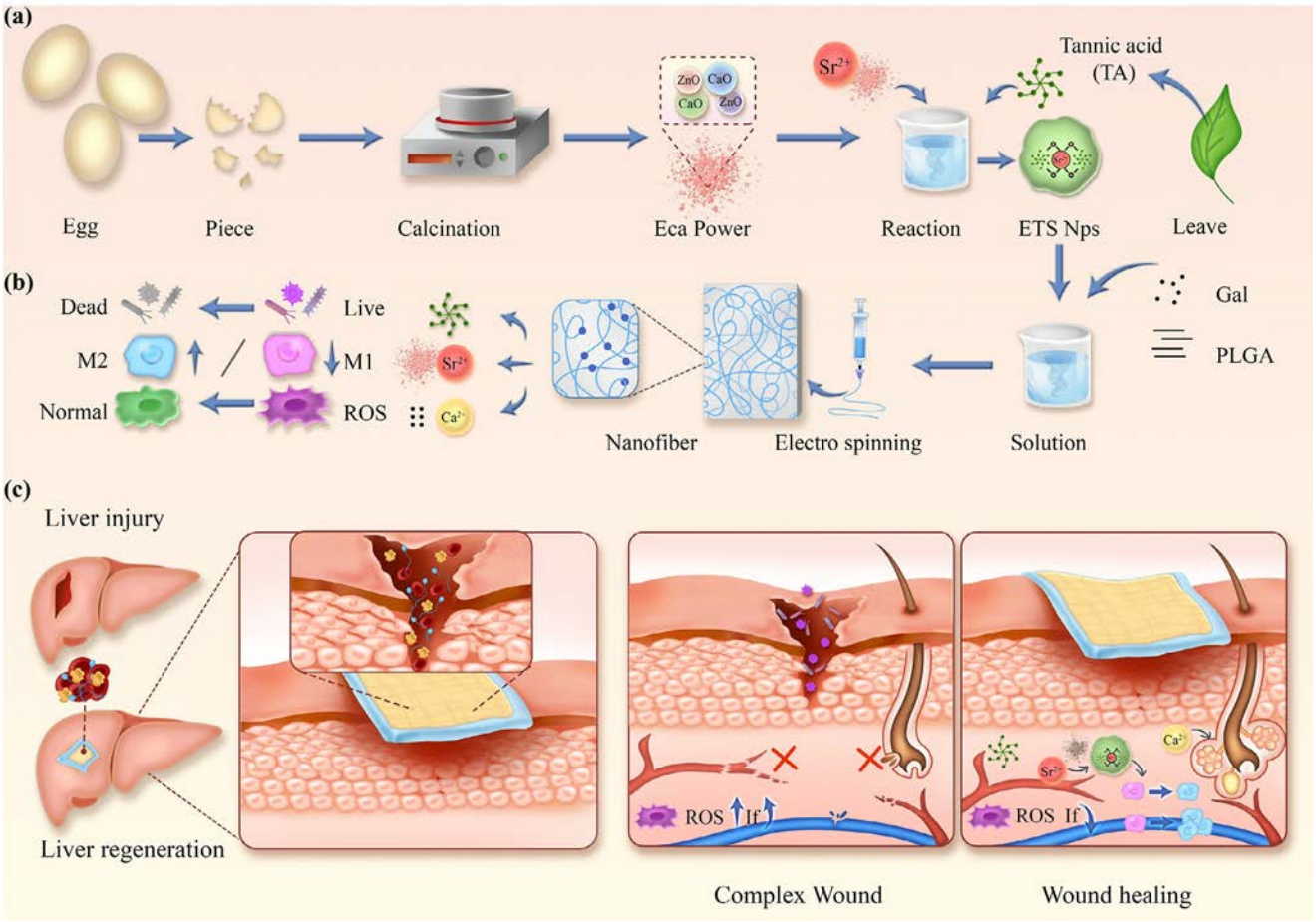

Figure 1. An overview of the experimental design. Synthesis of ECa-TA-Sr NPs (a) and nanofiber scaffolds containing ECa-TA-Sr NPs (b). Illustration of the potential mechanism of scaffolds for hemostasis and wound healing (c).

suggestive of the good hydrophilicity of membranes (Figure S4, Supporting Information). The hydrophilicity of membranes can be ascribed to the Gel (Figure 2d).

To delineate whether NPs were successfully loaded into fibers, as well as discern the dispersion of NPs into fibers, we carried out EDS analysis. EDS mapping showed the lack of calcium (Ca) and strontium (Sr) elements in the PG group. On the other hand, the PG-ETS group, which was loaded with ECa-TA-Sr NPs, exhibited Ca and Sr elements with good dispersibility. PG-E and PG-ET groups also displayed Ca element with good dispersibility (**Figure 3a**; Figure S5, Supporting Information). These data showed that the NPs can be uniformly loaded in fibers with an insignificant difference in the fibers' morphology.

Scaffold materials should also exhibit degradation rate commensurate with the neo-tissue regeneration. The degradation of the scaffold may also help obtain the sustained and controlled release of bioactive components.[21] The remaining mass of scaffolds after degradation was gradually decreased with an increase in degradation time (Figure S5, Supporting Information). Moreover, morphological analysis with SEM revealed that the fibers were gradually broken in all scaffolds with an increase in the degradation time for up to day 21 (Figure 3b; Figures S6 and S7, Supporting Information). The values for the remaining mass were 47.7 ± 5.9%, 42.9 ± 5.1%, 43.8 ± 3.4%, and 42.5 ± 2.9% for PG, PG-E, PG-ET, and PG-ETS groups, respectively (Figure 3e).

TA has a significant anti-oxidative function. We carried out DPPH assay to delineate anti-oxidative properties of TA-loaded membranes. Optical photographs showed less intense colour of PG-E and PG-ET groups than that of other groups, which may be attributed to the TA (Figure 3e). The values for anti-oxidative ratio were found to be 13.7 ± 1.5%, 13.0 ± 2.7%, 50.3 ± 2.1%, and 50.3 ± 3.7% for PG, PG-E, PG-ET, and PG-ETS groups, respectively (Figure 3d). These data showed anti-oxidative ability of TA-loaded fibers.

2.2. Biocompatibility and Biofunction Assay In Vitro

Trauma often results in the exudation of blood; thus, hemocompatibility and hemostatic ability of dressings should be additionally considered for wound healing.[12] As shown in Figure S8a,b (Supporting Information), the test solution of hemolysis assay showed slight light red color after centrifugation, and the hemolysis rate was 1.52 ± 0.34%, 0.23 ± 0.19%, 1.12 ± 0.55%, 1.69 ± 0.34%, and 1.66 ± 0.44% for gauze, PG, PG-E, PG-ET, and PG-ETS groups, respectively. These results showed that the hemol-

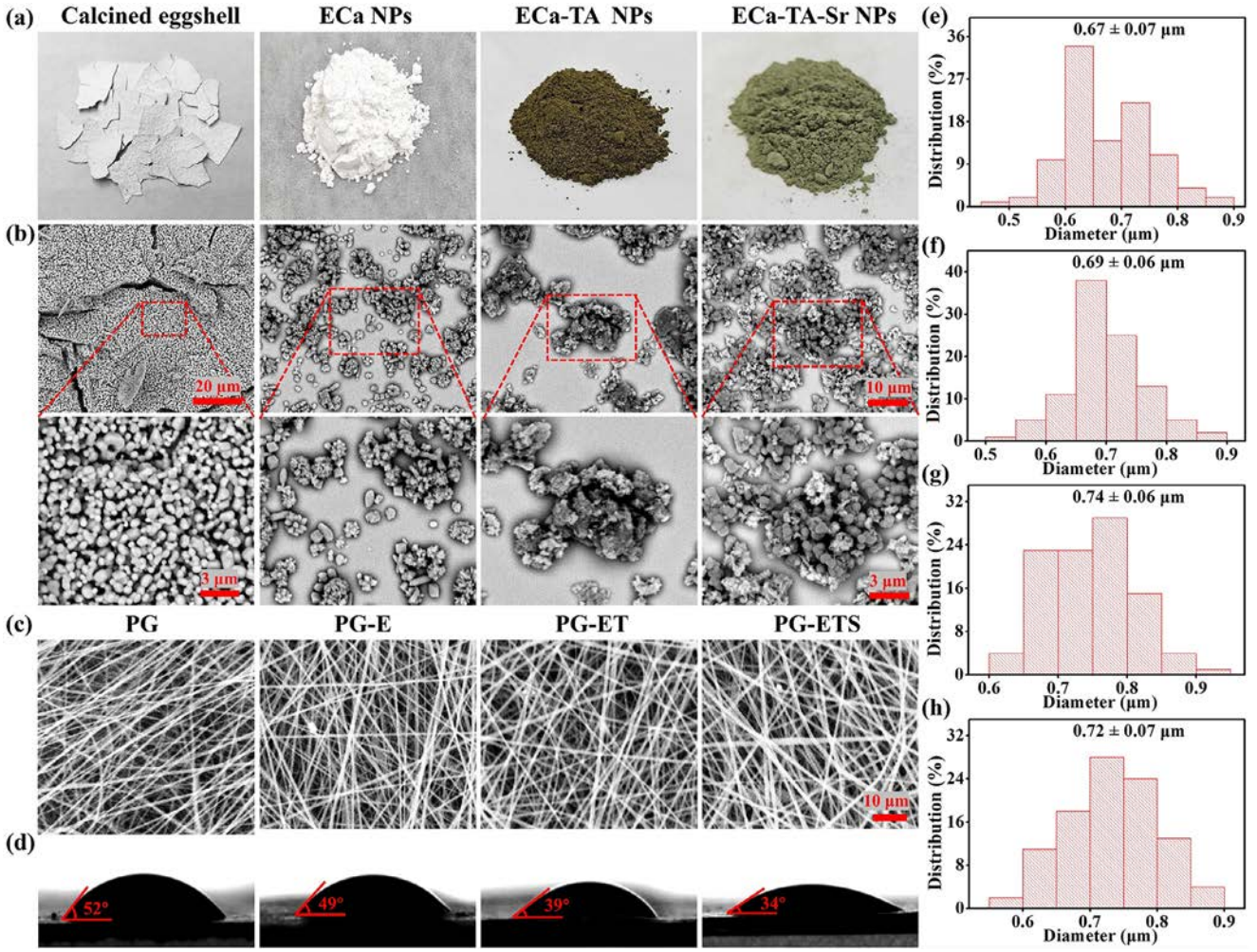

Figure 2. Characterization of NPs and scaffolds. Optical photographs a) and SEM photomicrographs b) of eggshell and different types of NPs. c) SEM images of various scaffolds. d) Water contact angle of scaffolds. e–h) Average fiber diameter distribution of e) PG, f) PG-E, g) PG-ET, and h) PG-ETS scaffolds.

ysis rate of all scaffolds was within the acceptable range (< 5%) for application of the biological materials, which indicated good hemocompatibility of membranes.

Moreover, the cytocompatibility of scaffolds was evaluated by CCK-8 assay and live/dead staining using HUVECs and NIH-3T3 fibroblasts. Both cell types showed distinct proliferation as evaluated for up to 5 days, thereby indicating the cytocompatibility of scaffolds (**Figure** 4a,b). Live/dead staining showed that most of the seeded cells were viable with only a few dead cells (Figure 4d,e). HUVECs are highly correlated with blood vessel regeneration, while NIH-3T3 fibroblasts are highly correlated with cell proliferation and tissue remodeling in wound healing.[23] These data showed that bioactive components from the scaffold may not interfere with the cytocompatibility of scaffolds. These bioactive components can promote cell survival as well as proliferation, which may have implications for tissue regeneration in vitro and in vivo.

Hemostatic ability of the scaffold can be preliminarily verified by coagulation in vitro. PG-E, PG-ET, and PG-ETS groups showed hemostatic ability and promoted blood clotting. The blood clotting index (BCI) values were 56.2 ± 2.2%, 62.7 ± 3.3%, 9.92 ± 2.08%, 2.22 ± 1.22%, and 4.18 ± 1.32% for PG, PG-E, PG-ET, and PG-ETS groups, respectively (Figure 4c). The surface of PG-E, PG-ET, and PG-ETS groups was covered with a large number of blood clots, while the surface of gauze and PG had no significant residual erythrocytes (Figure S9, Supporting Information). These data showed that the bioactivity of ECa NPs, ECa-TA NPs, and ECa-TA-Sr NPs was remained preserved, which can promote blood clotting even after incorporation into fibers.

Since cell migration plays a pivotal role in accelerating tissue repair, we ascertained the migration of HUVECs and NIH-3T3 fibroblasts with a Transwell migration assay in vitro.[24] PG-E, PG-ET, and PG-ETS groups promoted the migration of both cell types, which can be ascribed to the ECa, TA, and strontium ions (Sr^{2+}) (**Figure** 5a,e). PG-ETS group also outperformed other groups in terms of cell migration in vitro as evaluated with a scratch wound healing assay of HUVECs (Figure 5b). The cell migration rate was found to be 78.1 ±1.3%, 80.7 ±1.8%, 88.4 ± 1.7%, 85.4 ±1.2%, and 90.3 ± 1.2% for PG, PG-E, PG-ET, and PG-ETS groups, respectively (Figure 5f).

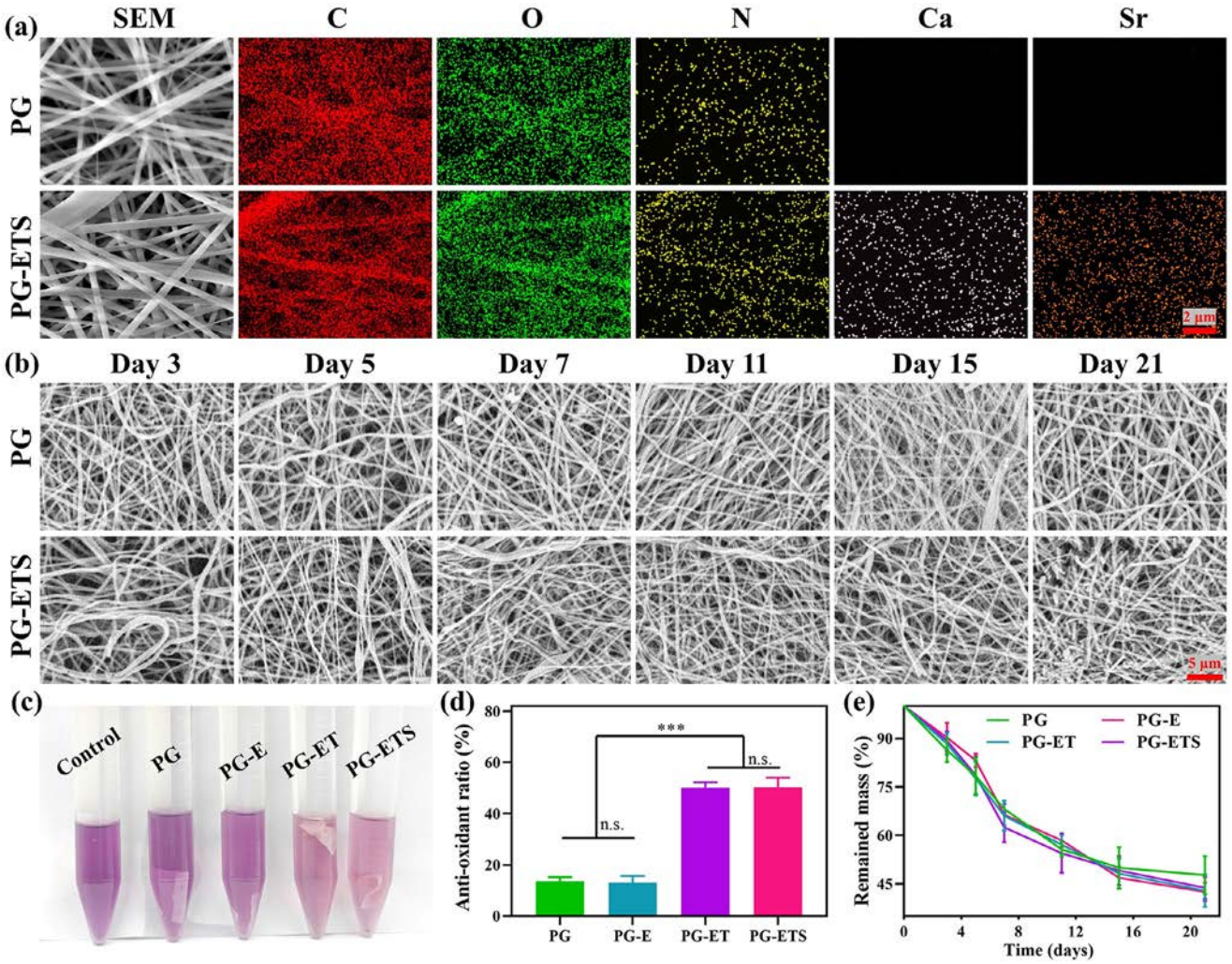

Figure 3. Characterization of scaffolds. a) SEM images and element mapping of PG and PG-ETS membrane. b) SEM micrographs of PG and PG-ETS membranes degraded at different time points in vitro. Optical photographs c) and DPPH assay d) of various scaffolds. e) The remaining mass of scaffolds degraded for up to different time points in vitro.

The tube-formation assays are widely used to evaluate the angiogenic ability of scaffolds in vitro.[25] PG-E, PG-ET, and PG-ETS groups showed significant angiogenesis than that of the control group (Figure 5c). Angiogenesis parameters, such as number of meshes were quantitatively measured with ImageJ. The number of meshes were found to be 4.50 ± 1.73%, 5.75 ± 1.26%, 10.0 ± 1.8%, 10.8 ± 1.5%, and 14.5 ± 1.3% for PG, PG-E, PG-ET, and PG-ETS groups, respectively (Figure 5c,g). These results indicated that ECa, TA, and Sr components can promote tubule-like network formation of HUVECs in vitro, which may have implications for the application of these dressings in vivo.

E. coli and *S. aureus* are widely used to discern antibacterial properties of biomaterials.[26] As shown in Figure 5d, PG-ET and PG-ETS groups exhibited considerable antibacterial activity than that of other groups. The survival ratio of *E. coli* was 100.0 ±11.8%, 125.9 ± 12.8%, 136.7 ± 11.4%, 10.8 ± 1.7%, and 11.4 ± 1.3%, while for *S. aureus* was 100.0 ± 8.5%, 128.3 ± 4.0%, 130.9 ± 8.4%, 20.1 ± 5.6%, and 18.9 ± 5.9% for PG, PG-E, PG-ET, and PG-ETS groups, respectively (Figure 5d,h). These results showed that TA has very good antibacterial properties, and its function is not lost despite being prepared as a particle coating and loaded in nanofibers.

2.3. Hemostatic Ability of Membranes In Vivo

Hemostatic ability of membranes was discerned in a liver injury model in vivo (**Figure 6**a). As shown in Figure 6c, the gauze did not stop bleeding even after applied for up to 45 s. For the PG group, the blood leakage was observed for up to 35 s. PG-E, PG-ET, and PG-ETS groups exhibited a shorter hemostasis time with a smaller area of bloodstains. Hemostaticis time was 56.0 ± 8.0, 40.3 ± 6.2, 22.5 ± 3.3, 19.8 ± 4.4, and 21.0 ± 1.6 s for control, PG, PG-E, PG-ET, and PG-ETS groups, respectively (Figure 6b). Thus, the PG-E, PG-ET, and PG-ETS groups also displayed hemostatic ability in vivo.

We further ascertained the biocompatibility of membranes in a liver injury model in vivo. All groups exhibited distinct

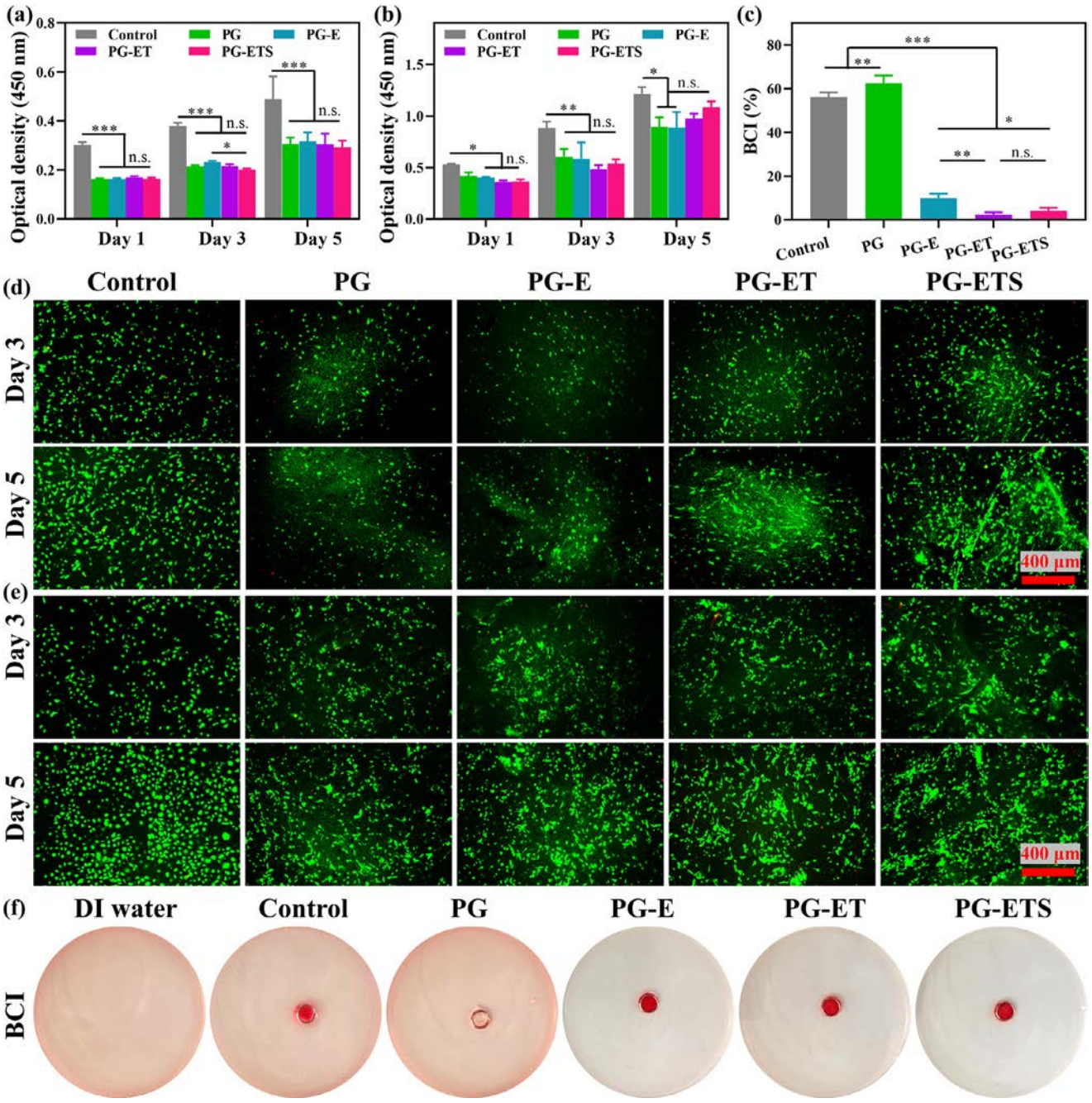

Figure 4. Cytocompatibility of different types of scaffolds. The CCK-8 assay for NIH-3T3 fibroblasts a) and HUVECs b) for up to 5 days in vitro. Quantitative analysis of blood clotting index (BCI) assay c). Live/dead staining of scaffolds either seeded with NIH-3T3 fibroblasts d) or HUVECs e) at day 3 and 5. Optical photographs of the scaffolds in a BCI assay f).

degradation along with the infiltration of surrounding tissues, which is indicative of the good biocompatibility of membranes in vivo (Figure S10a, Supporting Information). PG-ET and PG-ETS groups showed more number of infiltrated cells per high power field (HPF) due in part to the release of active ingredients from scaffolds, which can promote cell proliferation and migration. The MT staining showed collagen deposition in all groups; the PG-ETS group outperformed other groups in terms of the collagen deposition (Figure S10b, Supporting Information). These beneficial effects can be ascribed to the release of Sr^{2+} from ECa-TA-Sr NPs, which can promote angiogenesis as well as downregulate the inflammatory environment, thereby promoting collagen deposition as well as maturation. Taken together, these scaffolds exhibited biocompatibility and biodegradability in vivo.

As shown in **Figure** 7a, the liver defect site achieved hemolysis, while the dressing was covered around the wound site to further delineate liver tissue regeneration. While normal liver tissues do not form adhesions to surrounding tissues, inflammatory cells

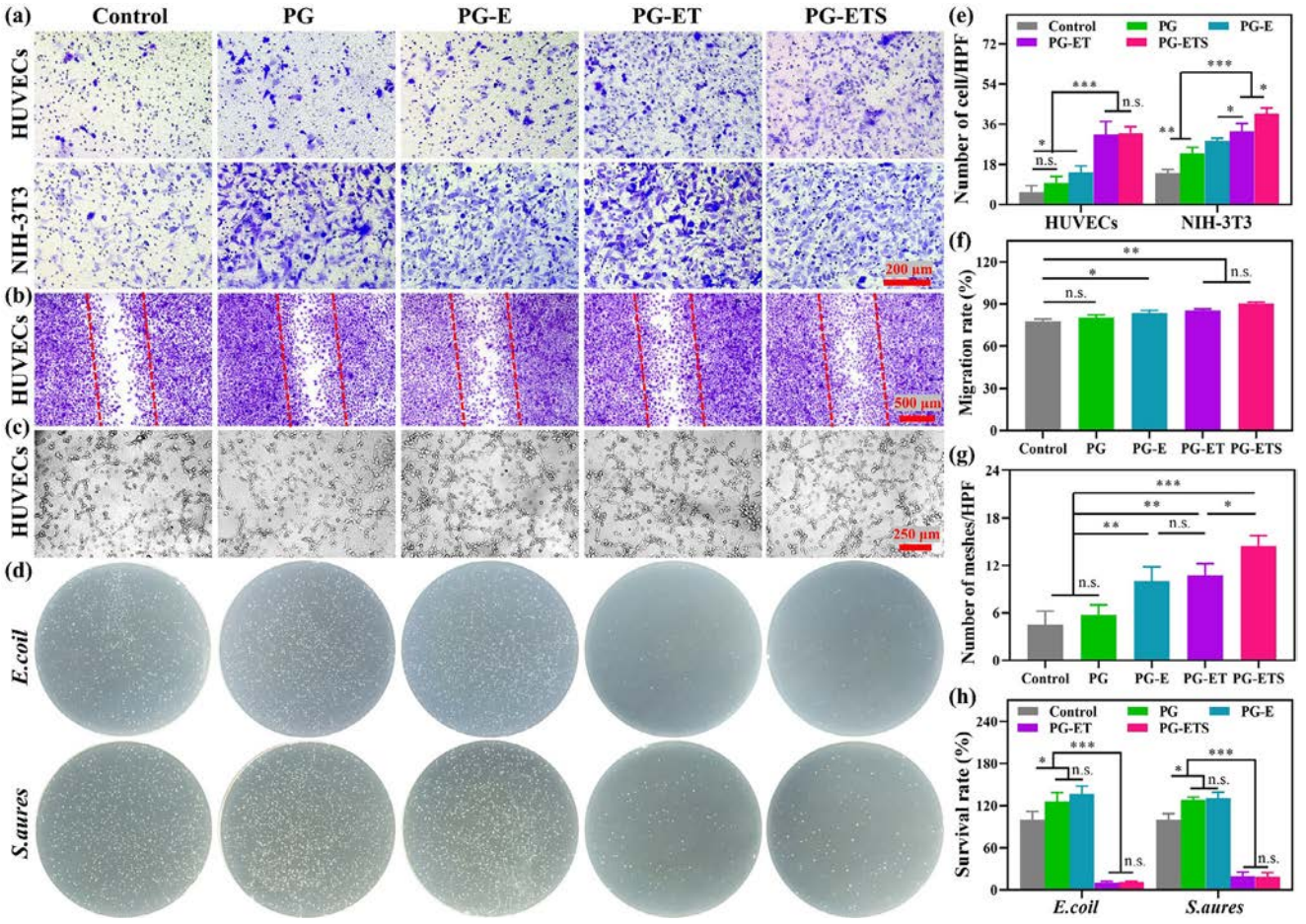

Figure 5. Biofunction assay of scaffolds in vitro. a) Transwell migration assay of scaffolds for HUVECs and NIH-3T3 fibroblasts at 12 h. b) The scratch wound healing for HUVECs at 24 h. c) The tube-formation assay for HUVECs at 6 h. d) Antibacterial activity for *E.coil* and *S.aures*. Quantitative analysis of cell migration for Transwell migration assay e) and scratch wound healing f). Number of meshes in the tube formation assay g). The survival ratio of *E. coli* and *S. aureus* h).

could aggregate and secrete inflammatory factors to promote an aggregation of fibroblasts to form adhesions after tissue injury (Figure 7b). The PG group showed a smaller amount of residue than that of other groups, which may be due to the lower degradation rate of the NPs, to delay the degradation rate of the scaffold in vivo. While PG-E group showed significant tissue adhesion, PG-ET and PG-ETS groups showed appreciably less adhesion with the surrounding tissues. The lower tissue adhesion in PG-ET and PG-ETS groups may be ascribed to the TA released from NPs, which can inhibit inflammation to avoid tissue adhesion.

H&E staining showed uniform distribution of hepatocytes accompanied by vascular tissue in the regenerated liver tissues (Figure 7c). The injured liver treated with PG exhibited a minimal amount of residual scaffold at the wound site along with infiltration of only a few numbers of host cells, which is indicative of the poor ability of the PG to regenerate the liver (Figure 7c). On the other hand, while the PG-E group showed significant cell infiltration at the wound site, it showed appreciable tissue adhesion. More importantly, both PG-ET and PG-ETS groups displayed significant infiltration of host cells as well as surrounding tissues at the injury site with negligible tissue adhesion, which may be ascribed to the TA. It is worth noting that the PG-ETS group outperformed other groups in terms of the host cell infiltration, which may have implications for the regeneration of the injured liver.

2.4. Wound Healing Assay In Vivo

We further elucidated the potential of scaffolds to improve wound healing in a full-thickness excisional defect model in SD rats for up to 14 days in vivo. The wound size was gradually decreased over a period of 14 days (**Figure** 8a). PG-ET and PG-ETS groups outperformed other groups in terms of skin tissue repair and exhibited rapid wound closure (wound healing rate, 84.9 ± 1.4%, 88.5 ± 0.6%, 93.9 ± 1.0%, 95.2 ± 0.6%, and 95.8 ± 0.9% for control, PG, PG-E, PG-ET, and PG-ETS groups, respectively) (Figure 8d,e). H&E staining showed an obvious crust layer and large number of inflammatory cells in the wound site at day 14 (Figure S11a, Supporting Information). Masson's trichrome (MT) staining revealed insignificant epithelialization at the wound site, while obvious granulation tissue formation in the PG-ETS group (Figure S11b, Supporting Information).

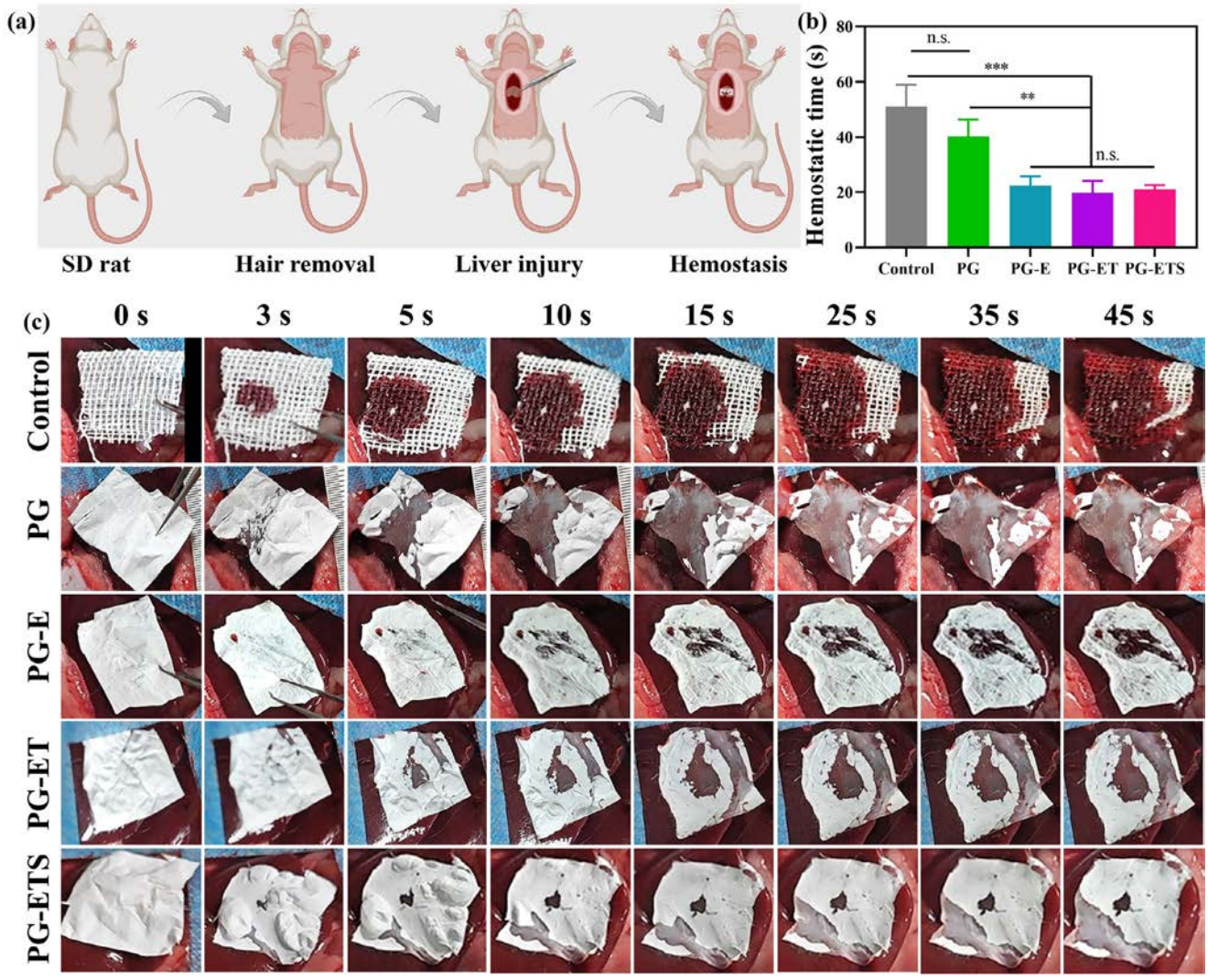

Figure 6. Hemostatic ability of membranes in a rat liver injury model. a) Schematic illustration of the evaluation of the hemostatic ability of scaffolds. b) The hemostatic time of various scaffolds. c) Optical photographs showing the treatment of the liver injury with scaffolds.

By day 14, PG-ET and PG-ETS groups exhibited epithelium regeneration alongside mild inflammation. Moreover, PG-ET and PG-ETS groups exhibited significantly less scar length as compared with the other groups at the wound site. The numbers of inflammatory cells was found to be 193.0 ± 35.4/HPF, 383.8 ± 37.2/HPF, 236.0 ± 27.4/HPF, 32.8 ± 3.9/HPF, and 21.0 ± 3.6/HPF or control, PG, PG-E, PG-ET, and PG-ETS groups at day 14, respectively. On the other hand, the scar length was 4.95 ± 0.19 mm, 3.91 ± 0.22 mm, 2.34 ± 0.17 mm, 2.25 ± 0.16 mm, and 1.33 ± 0.17 mm for control, PG, PG-E, PG-ET, and PG-ETS groups at day 14 post-operatively, respectively (Figure 8f,g). MT staining showed considerable collagen deposition in the PG-ETS group than that of the other groups (Figure 8c). Moreover, there were obvious glands, hair follicles, and other skin appendages around the wound site in PG-E, PG-ET, and PG-ETS groups (Figure S12, Supporting Information). These results indicated that the ECa NPs can promote the reconstruction of skin appendages, which may have implications for a high-quality skin repair. Moreover, the PG-ETS group outperformed other groups in terms of skin tissue repair, which may be ascribed to the synergistic effect of ECa, TA, and Sr^{2+}.

3. Discussion

With the development of TE, different types of dressings have been developed for skin tissue repair.[27] Successful skin repair should consider various factors, including hemostatic ability of dressings, antibacterial properties, and anti-inflammatory potential.[28] ECa NPs with excellent hemostatic ability as well as ECM production ability were successfully employed for tissue repair.[10] The ECa NPs are derived from ES; the latter belongs to the byproducts of food industries and other consumptions, which can be regarded as a benign, sustainable resource of the Ca and can be prepared into different types of bioactive materials, thereby acting as a valuable feedstock for the circular economy.

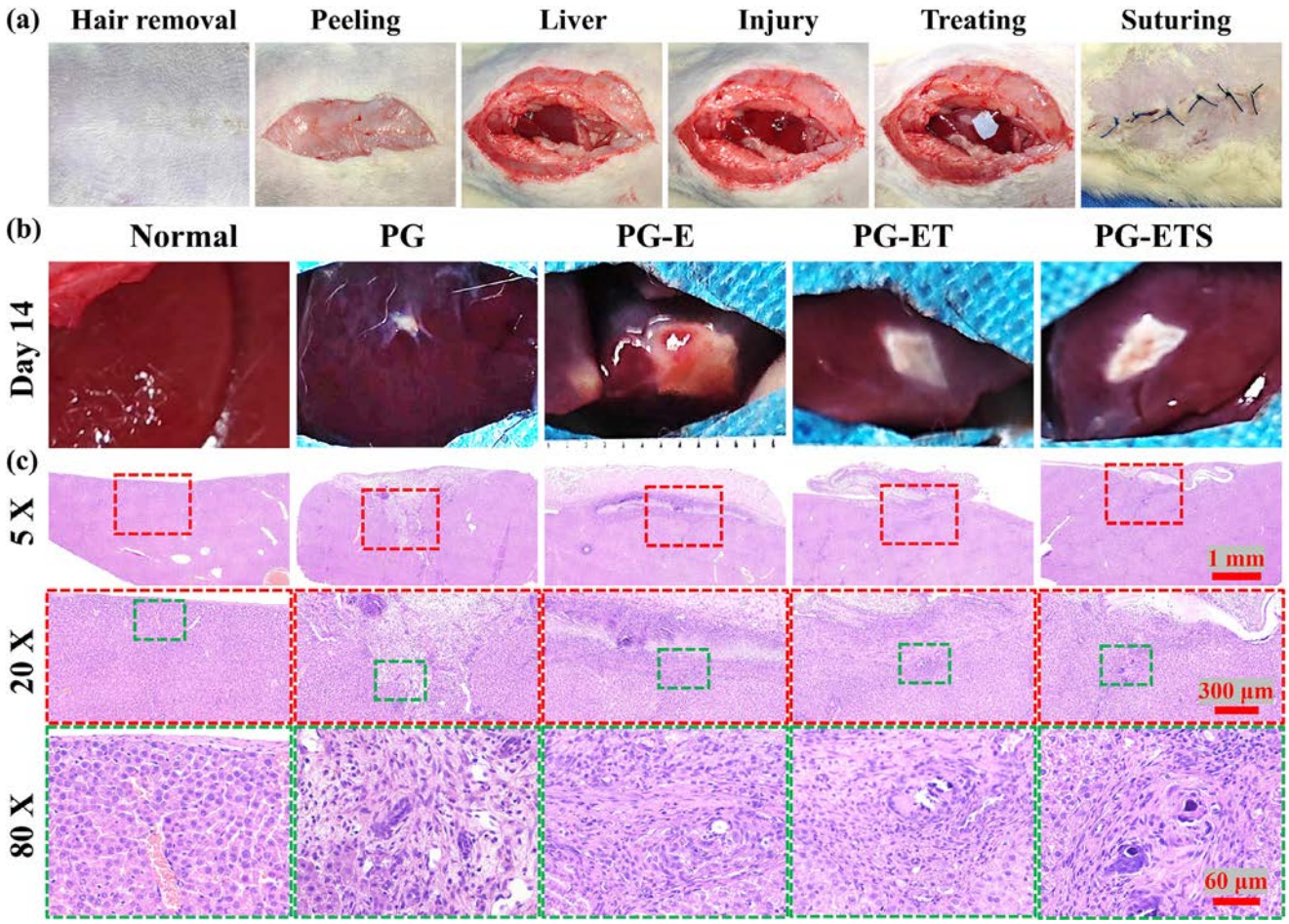

Figure 7. Preparation of liver injury model and its treatment process with different types of dressings a). Photographs showing the treatment of liver injury with various scaffolds for up to day 14 b). H&E staining of regenerated liver tissues at day 14 c).

Residual organic impurities of the ES could be removed by high-temperature calcination to obtain ECa NPs. ECa NPs also retain additional metal oxides, such as magnesium oxide (MgO) and silicon oxide (SiO_2), which may show different types of biological functions.[10] Calcium (Ca), magnesium (Mg), and silicon (Si) elements can release their corresponding ions for wound hemostasis, cell proliferation, and ECM production.[29] Moreover, magnesium (Mg) and silicon (Si) can also play a pivotal role in simultaneous osteogenesis and angiogenesis. Therefore, ECa NPs may exhibit considerable application prospects for soft and hard tissue repair.[30]

While ECa exhibits various biological functions, it is still necessary to impart additional biological functions to wound dressings, such as antibacterial, anti-inflammatory, and angiogenic properties, for an effective skin tissue repair.[31] TA has antibacterial, anti-inflammatory, and anti-oxidative functions. Moreover, Sr^{2+} displays beneficial angiogenic functions. Therefore, to harness the multifunctional benefits of ECs alongside TA and Sr^{2+}, we fabricated ECa-TA-Sr NPs (Figure 1a). Further, to stabilize the application form of NPs, they were loaded into fibers to obtain different types of dressings by electrospinning. These dressings showed good air permeability, hydrophilicity, and degradation characteristics, which may have implications for achieving the release of bioactive ingredients during wound application.[32] We and other researchers have used a 7:3 (w/w) ratio of PLGA and Gel to fabricate wound dressings. It is worth noting that dressings prepared using this composition of PLGA/Gel exhibit good structural stability with appreciable mechanical properties and good biocompatibility.[23]

These dressings showed good biocompatibility as well as biological functions, such as anti-oxidative ability, antibacterial ability, and angiogenic network formation (Figure 4). We envision that the TA component of NPs can impart antibacterial function to the membranes as follows: *i*) The phenolic hydroxyl (-OH) groups in TA display free radical scavenging ability upon their interaction with reactive oxygen species (ROS). Moreover, TA can inhibit lipid peroxidation.[33] *ii*) The TA can chelate metal ions to prevent the catalytic effect of metal ions on free radical generation and chain reaction.[34] *iii*) The TA also exhibits an inhibitory effect on certain oxidases, such as xanthine oxidase and tyrosinase, to reduce free radical production.[35] Dressings containing TA also significantly inhibited microbial growth (Figure 5d). The TA can bind to proteins or polysaccharides bacterial surface, thereby disrupting bacterial membranes as well as affecting the normal physiological functions of bacteria.[36] Meanwhile, Sr^{2+} also possesses antibacterial function due in part to its

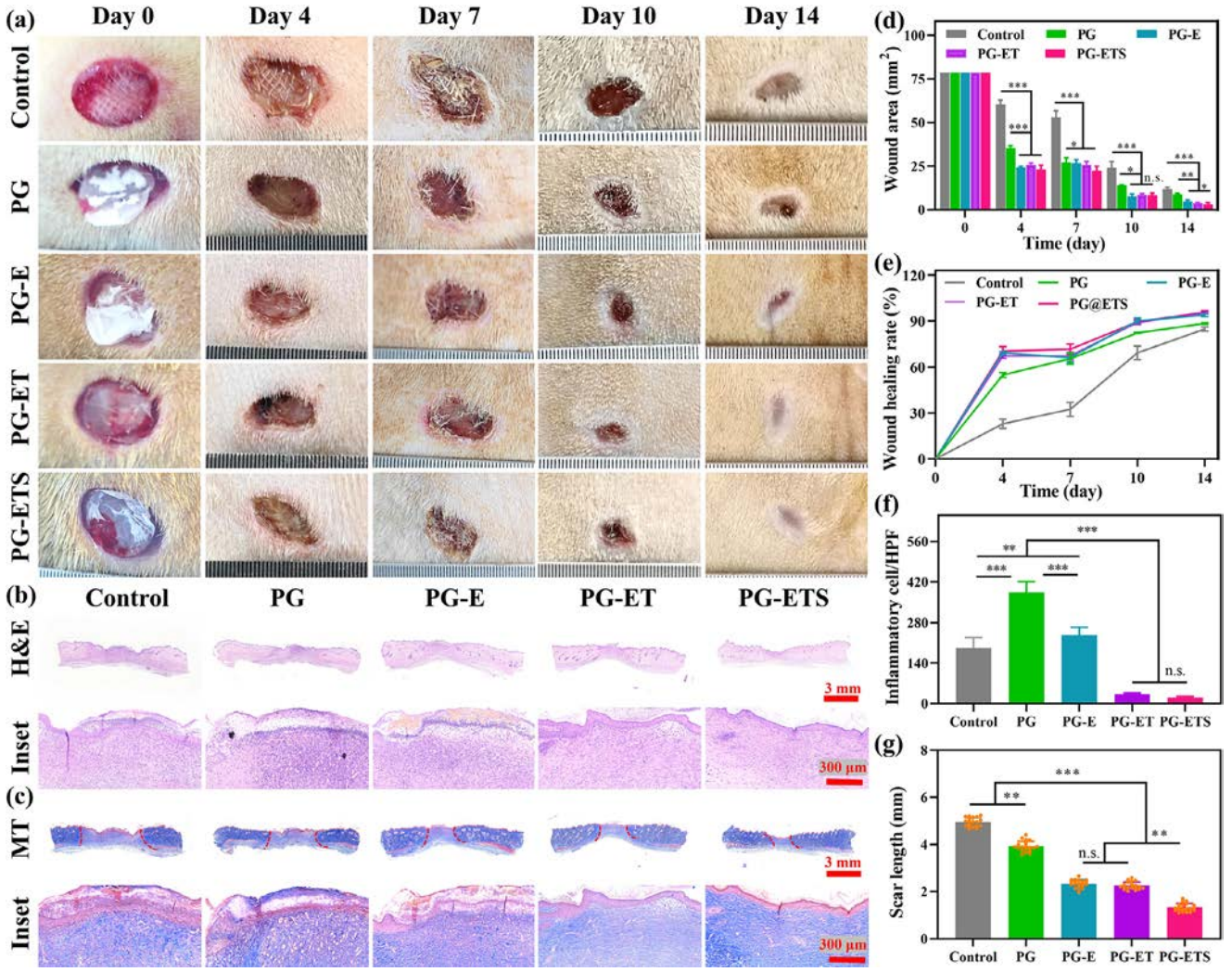

Figure 8. Wound healing potential of scaffolds in a full-thickness excisional defect model in SD rats. a) Optical photographs of the regenerated skin tissues treated with different types of scaffolds for up to day 14. H&E staining b) and MT staining c) of repaired skin tissues. Wound area d) and wound healing e) at each time point normalized with respect to day 0. The number of inflammatory cells f) and scar length g) at the wound site at day 14.

ability to destroy bacterial cell membranes, thereby further interfering with the metabolic process of bacteria to either inhibit or kill the bacteria.[37]

The TA further manifests anti-inflammatory function, which can regulate cytokine expression to reduce the occurrence of low-grade inflammatory diseases.[38] In addition, TA can inhibit the ability of lipopolysaccharides (LPS) to induce nitric oxide (NO) production in RAW264.7 macrophages.[39] Meanwhile, it has been shown that TA and Sr^{2+} can regulate the proportion of pro-inflammatory cells and inhibit the release of pro-inflammatory factors, including TNF-α and IL-6.[40] Besides, TA can promote the polarization of macrophages from M1 to M2 phenotype and release anti-inflammatory factors, including interleukin-10 (IL-10), which may in turn promote tissue regeneration.[35]

The pro-angiogenic effect of dressings in the PG-ETS group is mainly ascribed to the biological functions of ECa and Sr^{2+} (Figure 5c). First, ECa contains calcium oxide (CaO) and trace amount of other metallic elements, including magnesium (Mg), iron (Fe), and silicon (Si). These metallic elements can upregulate the expression of angiogenesis-related genes, including vascular endothelial growth factor (VEGF). These angiogenic genes can promote the proliferation, migration, and adhesion of vascular cells, thereby promoting the regeneration of arterioles and capillaries. The Sr^{2+} could further support the angiogenic functions of ECa by enhancing the proliferation and migration of ECs. Therefore, the PG-ETS group exhibited a significant angiogenesis effect as evaluated in a tube formation assay and scratch wound healing assay in vitro.

The PG-ETS group also showed good hemostatic ability as well as liver tissue regeneration with minimal tissue adhesion in a rat liver trauma model in vivo (Figure 6c). The PG-ETS group showed rapid hemostatic ability (≈20s). In comparison, chitosan-based hydrogels have been shown to exhibit longer hemostatic time (>30 s) alongside massive blood loss.[41] Upon tissue injury, inflammatory factors are accumulated at the injury site, which may induce an aggregation of fibroblasts, thereby leading to scar

tissue formation.[23] Moreover, excessive inflammation at injury site may cause uncontrolled growth of fibroblasts as well as severe tissue adhesion at the injury site, thereby precluding the recovery of lost tissue function at the wound site.[20] PG-ETS can accelerate liver tissue repair with negligible tissue adhesion, which is indicative of the promise of these dressings for liver tissue regeneration.[41,42]

The higher hemostatic ability of these dressings could be ascribed to the hydrophilicity, which can help increase blood absorption to form physical barriers and prevent bleeding at the injury site.[41] Second, TA can promote blood clotting via an interaction of the phenolic hydroxyl (-OH) groups with the blood; the polyphenol groups of the TA can also firmly attach to proteins and peptides.[43] Third, ECa can release therapeutic ions, such as calcium ions (Ca^{2+}), magnesium ions (Mg^{2+}), and silicon ions (Si^{4+}); these metallic ions can promote intrinsic and extrinsic coagulation pathways, and further augment platelet activation and aggregation by the protein kinase C (PKC) pathway for rapid hemostatic ability.[44] PG-ETS dressings additionally exhibited anti-inflammatory properties to inhibit excessive aggregation of fibroblasts. Besides, dressings can resolve inflammation, increase the proliferation of hepatocytes, and induce ECM production and/or matrix secretion, thereby weakening tissue adhesion.[39] PG-ETS dressings also exhibited rapid wound closure (96% wound closure rate). In comparison, hydrogel dressings, such as gelatin/oxidized dextran hydrogels, have been shown to exhibit wound closure rate for up to 88% by day 14.[45,46] Rapid wound closure of PG-ETS dressings may be ascribed to their ability to facilitate wound healing, due in part to the different types of factors.

The PG-ETS can rapidly achieve hemostasis, which may in turn promote the transition of the inflammatory stage in wound healing. Second, TA and Sr^{2+} could downregulate the level of inflammation as well as suppress microbial growth and scavenge ROS at the injury site, thereby providing a stable microenvironment for wound regeneration. Third, Sr^{2+} can promote angiogenesis, while ECa NPs can promote the proliferation of fibroblasts as well as the production of collagen from fibroblasts to induce skin repair. The Sr^{2+} can promote blood vessel formation, which may further help promote timely wound healing as well as increase the diffusion of oxygen as well as the transport of nutrients. Taken together, PG-ETS dressings may possess broad implications for hemostatic and skin repair.

4. Conclusion

ES was prepared into ECa-TA-Sr NPs. These NPs were further prepared into PG-ETS dressings. These dressings showed multifunctional characteristics, such as rapid hemostatic ability in a rat liver trauma model, antibacterial properties against *E. coli* and *S. aureus*, anti-inflammatory ability, angiogenic network formation of HUVECs, and so on. Morphological analysis of fibers showed that the ECa-TA-Sr NPs can be successfully loaded into fibers. The biocompatibility and biological function assay further showed good cytocompatibility and hemocompatibility of dressings. PG-ETS dressing also showed faster hemostasis (blood clotting time, ≈20 s) and additionally promoted liver tissue regeneration. PG-ETS dressings also enabled the regeneration of full-thickness excisional defects in a rat model with mild inflammation and epithelial tissue regeneration. Taken together, ECa-TA-Sr NPs derived from the ES may endow multifunctionality to dressings, which may have the potential to promote soft tissue repair and other related disciplines.

5. Experimental Section

Materials: Eggs were purchased from the Shanghai Yonghui Supermarket (Shanghai, China). Egg shells were prepared by removing the egg white and egg membrane. Poly(lactic acid) (PLA, M_n = 300 kDa) and Gelatin (Gel) were obtained from Medprin Regenerative Medical Technologies Co., Ltd (Shanghai, China) and MP Biomedicals, LLC (Shanghai, China), respectively. NIH-3T3 fibroblasts and human umbilical vein endothelial cells (HUVECs) were obtained from the Typical Culture Collection Committee Cell Bank (Shanghai, China).

Fabrication of Nanoparticles and Scaffolds—Synthesis of Nanoparticles: To obtain ECa, the eggshell (ES) was calcined in a muffle furnace (Yamato Scientific Co., Ltd, FO711, Shanghai, China) at 1000 °C for 3 h. The calcined ES was ground to obtain ECa NPs. To remove larger particles, ECa powder was dispersed in absolute ethanol and filtered with 1,800 mesh screens to obtain particles with a size smaller than that of 10 µm. ECa powder was freeze-dried to obtain ECa NPs.

To obtain TA-modified ECa NPs (ECa-TA Nps), 1 mg of TA and 10 mg of ECa NPs were dispersed into 100 mL of water. To preserve the activity of TA as well as the stability of Sr^{2+} during the synthesis of NPs, the pH of the solution was adjusted to 4.35 with HCl (0.1 M), which may also be beneficial for stable coating.[47] The reaction was carried out at 30 °C at 700 rpm for 10 min.[47] To obtain strontium (Sr)-substituted ECa-TA Nps (ECa-TA-Sr NPs), 1 mg of TA, 10 mg of ECa NPs, and 200 mM strontium chloride ($SrCl_2$) were dispersed into 100 mL of water. The pH of the solution was adjusted to 4.35 with HCl (0.1 M). The reaction was carried out at 30 °C for 10 min at 700 rpm. ECa-TA and ECa-TA-Sr NPs were collected by centrifugation at 4000 rpm for 10 min at room temperature (r.t.). The particles were obtained by freeze-drying.

Fabrication of Nanoparticles and Scaffolds—Fabrication of Scaffolds: To prepare scaffolds, PLA (0.7 g) and Gel (0.3 g) were dissolved in 10 mL of 1,1,1,3,3,3- hexafluoro-2-propanol (HFIP) to obtain 10% (w/v) PG solution. 1 mg ECa, ECa-TA, and ECa-TA-Sr NPs were added into the PG solution to obtain PG-E, PG-ET, and PG-ETS solutions, respectively. Fibers were prepared using electrospinning (Yongkang Leye Technology Development Co., Ltd. SS-3556H, Beijing, China) using these parameters: applied voltage, 12 kV, flow rate, 1.5 mL h^{-1}, and electrospinning time, 3 h.

Physicochemical Analysis: Morphological analysis and elemental mapping of scaffolds were carried out with scanning electron microscopy (SEM, Hitachi, TM-1000, Tokyo, Japan) and energy-dispersive X-ray spectroscopy (EDS). Moreover, ECa NPs were subjected to EDS testing for elemental analysis. The porosity of PG-ETS scaffolds (δ, 0.30 mm; Φ, 30 mm) was measured with a CFP-1100-AI capillary flow porometer (PMI Porous Materials Inc., Ithaca, NY, USA). Hydrophilicity of scaffolds was ascertained with water contact angle measurement (WCA, DSA 100, Krüss, Hamburg, Germany).

For DPPH assay, 4 mL of DPPH solution (0.1 mmol L^{-1}) and samples (δ, 0.30 mm; 10 mm × 10 mm) were respectively placed into a 15 mL centrifuge tube under light protection. After 30 min, 100 µL of the solution was collected and absorbance was measured at 517 nm. The DPPH testing solution without the sample was regarded as a control group. The antioxidative ability of scaffolds was calculated by Equation (1):

$$\text{Anti} - \text{oxidant ratio} = \frac{(A_C - A_t)}{A_c} \times 100\% \quad (1)$$

The A_c and A_t represent the OD value of the DPPH solution (Control) and the sample, respectively.

For the degradation of scaffolds, samples (δ, 0.30 mm; Φ, 10 mm) were placed into a 3 mL centrifuge tube along with 2 mL of PBS (pH = 7.28 ± 0.01) for up to 21 days (temperature, 37 °C and 120 rpm). At corre-

sponding time points (3, 5, 7, 11, 15, 21 days), samples were rinsed with deionized water, vacuum dried, and weighed (W_t). The original weight was recorded as W_0. The morphology of degraded samples was observed by SEM. The residual mass of the scaffolds was calculated using Equation (2):

$$\text{Remaining } mass = \frac{W_t}{W_0} \times 100\% \quad (2)$$

Biocompatibility and Biological Functions of Membranes In Vitro: For biocompatibility and biological functions of scaffolds, different types of assays were carried out in vitro, such as cytocompatibility, hemolysis ratio, Transwell migration assay, scratch wound healing assay, tube formation assay, BCI assay, and antibacterial activity in vitro. The detailed methods are provided in the Supporting Information.

Animal Experiments: Animal experiments were approved by the Animal Care Committee of Binzhou Medical University Hospital, Shandong, China (Approval # 20250107–95).

Animal Experiments—Hemostasis of Scaffolds in a Liver Injury Model In Vivo: For liver injury model, SD rats (male, 8 weeks old) were anesthetized using IV administration of sodium pentobarbital (45 mg·kg^{-1}). The abdomen of the rats was shaved for surgical procedures. The liver was exposed and defects (Φ, 3 mm and δ, 2 mm) were created. The gauze (for the control group) or dressings (25 mm × 25 mm; thickness = 0.15 mm) were covered on the defect site. To further elucidate the regenerative performance of dressings, the implantation was carried out for up to 14 days. The repaired liver, along with the surrounding tissues, was harvested and stained with hematoxylin and eosin (H&E).

Animal Experiments—Wound Healing In Vivo: SD rats (n = 8, male, 6-week-old) were anesthetized using IV administration of sodium pentobarbital (45 mg·kg^{-1}). Full-thickness excisional defects (Φ = 10 mm) were created on the dorsal side, and scaffolds (e.g., gauze, PG, PG-E, PG-ET, PG-ETS, etc.) were implanted on the defect site. Wounds were covered with an elastic bandage to avoid the removal of the dressings. Photographs were collected at different time points. At days 7 and 14, the repaired skin along with the surrounding tissues was harvested, and stained with H&E and Masson's trichrome (MT). Scar length refers to the length of the fibrotic zone based on MT staining and was calculated by ImageJ (n = 30). The wound area was calculated with Image J (NIH, v1.8.0, USA). Wound healing rate was calculated by Equation (3):

$$\text{Wound healing rate} = \left(\frac{E_0 - E_t}{E_0}\right) \times 100\% \quad (3)$$

where E_0 and E_t indicate the wound size at day 0 and at the respective time points.

Supporting Information

Supporting Information is available from the Wiley Online Library or from the author.

Acknowledgements

B.S. and Z.Y. contributed equally to this work. The part of this research was funded by the Natural Science Foundation of Shandong Province (ZR2020QH071) and the Science and Technology Commission of Shanghai Municipality, China (20DZ2254900), the Sino German Science Foundation Research Exchange Center, China (M-0263). This project was also supported byOngoing Research Funding program, (ORF-2025-769), King Saud University, Riyadh, Saudi Arabia.

Conflict of Interest

The authors declare no conflict of interest.

Data Availability Statement

The data that support the findings of this study are available from the corresponding author upon reasonable request.

Keywords

eggshell, electrospinning, hemostasis, nanofiber membrane, nanoparticles, wound healing

Received: June 14, 2025
Revised: July 22, 2025
Published online: August 5, 2025

[1] Z. Li, S. Chen, B. Wu, Z. Liu, L. Cheng, Y. Bao, Y. Ma, L. Chen, X. Tong, F. Dai, *ACS Biomater. Sci. Eng.* **2020**, *6*, 6949.
[2] J. Li, F. Yu, G. Chen, J. Liu, X. L. Li, B. Cheng, X. M. Mo, C. Chen, J. F. Pan, *ACS Appl. Mater. Interfaces* **2020**, *12*, 2023.
[3] M. Yin, J. Wu, M. Deng, P. Wang, G. Ji, M. Wang, C. Zhou, N. T. Blum, W. Zhang, H. Shi, N. Jia, X. Wang, P. Huang, *ACS Nano* **2021**, *15*, 17842.
[4] T. Mehrabi, A. S. Mesgar, Z. Mohammadi, *ACS Biomater. Sci. Eng.* **2020**, *6*, 5399.
[5] M. Shafiq, L. Wang, D. Zhi, Q. Zhang, K. Wang, L. Wang, D. H. Kim, D. Kong, S. H. Kim, *J. Biomed. Mater. Res. – Part B Appl. Biomater.* **2019**, *107*, 1669.
[6] C. T. Turner, M. Hasanzadeh Kafshgari, E. Melville, B. Delalat, F. Harding, E. Mäkilä, J. J. Salonen, A. J. Cowin, N. H. Voelcker, *ACS Biomater. Sci. Eng.* **2016**, *2*, 2339.
[7] X. Han, S. Chen, Z. Cai, Y. Zhu, W. Yi, M. Guan, B. Liao, Y. Zhang, J. Shen, W. Cui, D. Bai, *Adv. Funct. Mater.* **2023**, *33*, https://doi.org/10.1002/adfm.202213008.
[8] K. Singh, V. B. Yadav, U. Yadav, G. Nath, A. Srivastava, P. Zamboni, P. Kerkar, P. S. Saxena, A. V. Singh, *Colloids Surf. A Physicochem. Eng. Asp.* **2023**, *670*, 131575.
[9] Z. Yuan, L. Zhang, S. Jiang, M. Sha, Y. Cai, Y. Chen, J. Song, X. Yu, H. Ijima, Y. Xu, X. Mo, *Smart Mater. Med.* **2023**, *4*, 407.
[10] Z. Yuan, S. Wu, L. Fu, M. Shafiq, Y. Liang, P. Li, X. Wang, H. Feng, R. Hashim, S. Lou, M. El-newehy, M. Moydeen, W. Zhang, X. Mo, S. Jiang, *Composites, Part B* **2025**, *292*, 112071.
[11] M. M. Pillai, R. Saha, P. Tayalia, *J. Mater. Sci.* **2023**, *58*, 6865.
[12] X. Zhao, C. Weng, H. Feng, M. Shafiq, X. Wang, L. Liu, L. Han, M. El-newehy, M. M. Abdulhameed, Z. Yuan, X. Mo, Y. Wang, *Mater. Today Bio* **2025**, *30*, 101408.
[13] V. Chandrasekar, A. J. Panicker, A. K. Dey, S. Mohammad, A. Chakraborty, S. K. Samal, A. Dash, J. Bhadra, M. Suar, M. Khare, S. P. Dakua, A. V. Singh, *Discov. Toxicol.* **2024**, *1*, 9.
[14] Z. Yuan, L. Zhang, M. Shafiq, X. Wang, P. Cai, A. Hafeez, Y. Ding, Z. Wang, M. El-newehy, M. Moydeen, L. Jiang, X. Mo, Y. Xu, *J. Colloid Interface Sci.* **2024**, *673*, 411.
[15] S. Bao, D. Yu, Z. Tang, H. Wu, H. Zhang, N. Wang, Y. Liu, H. Huang, C. Liu, X. Li, Z. Guo, *Bioact. Mater.* **2024**, *34*, 64.
[16] S. Mcloughlin, A. R. Mckenna, J. P. Fisher, *ACS Appl. Bio Mater.* **2023**, *6*, 2546.
[17] S. D. Aker, S. Tamburaci, F. Tihminlioglu, *ACS Omega* **2023**, *8*, 19674.
[18] A. Li, X. Zeng, B. Yin, Y. Liang, X. Dong, Q. Bai, Z. Pan, L. Wang, L. Zhang, M. Yang, Y. She, W. Sun, K. Zhang, C. Chen, *Nat. Commun.* **2025**, *16*, 5734.
[19] C. Liu, X. Xu, W. Cui, H. Zhang, *Eng. Regen.* **2021**, *2*, 105.
[20] A. V. Singh, D. Gemmati, A. Kanase, I. Pandey, V. Misra, V. Kishore, T. Jahnke, J. Bill, *Veins Lymphatics* **2018**, *7*, 7196.

[21] S. Tomar, R. Pandey, P. Surya, R. Verma, R. Mathur, G. Gangenahalli, S. M Singh, *ACS Biomater. Sci. Eng.* **2023**, *9*, 1520.
[22] F. Carton, M. Malatesta, *Int. J. Mol. Sci.* **2024**, *25*, 3675.
[23] Z. Yuan, M. Shafiq, H. Zheng, L. Zhang, Z. Wang, X. Yu, J. Song, B. Sun, M. El-newehy, *Mater. Des.* **2023**, *235*, 112459.
[24] G. Cai, Z. Yuan, X. Wang, S. Wu, S. Zhou, Z. Lei, *Chem. Eng. J.* **2024**, *500*, 156555.
[25] Z. Yuan, D. Sheng, L. Jiang, M. Shafiq, A. ur Rehman Khan, R. Hashim, Y. Chen, B. Li, X. Xie, J. Chen, Y. Morsi, X. Mo, S. Chen, *Acta Biomater.* **2022**, *140*, 233.
[26] Z. Ming, L. Han, H. Zhu, M. Bao, Q. Fan, S. Xue, K. Wang, Y. Zhang, M. Lu, C. Xu, Q. Wu, T. Li, F. Sun, *Chem. Eng. J.* **2023**, *465*, 142889.
[27] D. Lin, M. Li, L. Wang, J. Cheng, Y. Yang, H. Wang, J. Ye, Y. Liu, *Adv. Funct. Mater.* **2024**, *34*, 2405255.
[28] X. Zhang, Y. Wu, H. Gong, Y. Xiong, Y. Chen, L. Li, B. Zhi, S. Lv, T. Peng, H. Zhang, *Small* **2024**, *20*, 2400516.
[29] X. Haixia, Z. Peng, L. Jiezhao, G. Huiling, C. Xie, W. Yihan, J. Yanglei, J. Li, C. Wang, X. Wenning, Z. Lixin, C. Liu, *ACS Appl. Mater. Interfaces* **2024**, *16*, 9626.
[30] L. Wang, Y. Qiu, Y. Guo, Y. Si, L. Liu, J. Cao, J. Yu, X. Li, Q. Zhang, *Nano Lett.* **2019**, *19*, 9112.
[31] Q. Tang, Q. Ke, Q. Chen, X. Zhang, J. Su, C. Ning, L. Fang, *ACS Appl. Mater. Interfaces* **2023**, *15*, 17641.
[32] W. Nie, E. J. Marrotte, R. Xie, H. G. Machens, A. F. Schilling, Y. Shen, M. Seeds, A. Atala, X. Dai, *Compos. Part B Eng.* **2025**, *291*, 111972.
[33] A. Capabilities, J. Wen, J. Tang, H. Ning, N. Hu, Y. Zhu, Y. Gong, C. Xu, Q. Zhao, X. Jiang, X. Hu, L. Lei, D. Wu, T. Huang, *Adv. Funct. Mater.* **2021**, *31*, 2011176.
[34] G. Pan, F. Li, S. He, W. Li, Q. Wu, J. He, R. Ruan, Z. Xiao, J. Zhang, H. Yang, *Adv. Funct. Mater.* **2022**, *32*, 2200908.
[35] M. Shafiq, Y. Chen, R. Hashim, C. He, X. Mo, X. Zhou, *Front. Bioeng. Biotechnol.* **2021**, *9*, 1.
[36] M. Feng, X. Zeng, Q. Lin, Y. Wang, H. Wei, S. Yang, G. Wang, X. Chen, M. Guo, X. Yang, J. Hu, Y. Zhang, X. Yang, Y. Du, Y. Zhao, *Adv. Healthcare Mater.* **2024**, *13*, 1.
[37] B. Pang, J. Xian, J. Chen, L. Ng, M. Li, G. Zhao, Y. E, X. Wang, X. Cao, C. Zhang, M. Zhang, C. Liu, *J. Funct. Biomater.* **2024**, *15*, 212.
[38] S. Jin, H. Jung, J. Song, S. Kim, S. Yoon, J. H. Kim, J. S. Lee, Y. J. Kim, D. Son, M. Shin, *Adv. Healthcare Mater.* **2025**, *14*, 2403722.
[39] W. Wei, J. Li, X. Han, Y. Yao, W. Zhao, R. Han, S. Li, Y. Zhang, C. Zheng, *Sci. Total Environ.* **2021**, *778*, 146189.
[40] Q. Hou, K. Liu, C. Lian, J. Liu, W. Wei, T. Qiu, H. Dai, *Biomacromolecules* **2023**, *24*, 3397.
[41] W. Wang, H. Yao, J. Xia, X. Wan, J. Wu, *Carbohydr. Polym.* **2025**, *353*, 123268.
[42] S. He, T. Walimbe, H. Chen, K. Gao, P. Kumar, Y. Wei, D. Hao, R. Liu, D. L. Farmer, K. S. Lam, J. Zhou, A. Panitch, A. Wang, *Bioact. Mater.* **2022**, *10*, 460.
[43] Q. Zhang, J. Zheng, L. Li, J. M. Yeh, X. Xie, Y. Zhao, C. Li, G. Hou, H. Yan, *Bioact. Mater.* **2025**, *46*, 173.
[44] J. Ma, C. Wu, *Exploration* **2022**, *2*, 20210083.
[45] Z. Cai, Q. Saiding, L. Cheng, L. Zhang, Z. Wang, F. Wang, X. Chen, G. Chen, L. Deng, W. Cui, *Bioact. Mater.* **2021**, *6*, 4506.
[46] B. Zhao, Y. Zhang, D. Li, X. Mo, J. H Pan, *Acta Biomater.* **2022**, *151*, 235.
[47] H. Byun, Y. Han, E. Kim, I. Jun, J. Lee, H. Jeong, S. J. Huh, J. Joo, S. R. Shin, H. Shin, *Bioact. Mater.* **2024**, *36*, 185.

